

NEW OBSERVATIONS OF $z \sim 7$ GALAXIES: EVIDENCE FOR A PATCHY REIONIZATION

L. PENTERICCI¹, E. VANZELLA², A. FONTANA¹, M. CASTELLANO¹, T. TREU³, A. MESINGER⁴, M. DIJKSTRA⁵, A. GRAZIAN¹,
M. BRADAČ⁶, C. CONSELICE⁷, S. CRISTIANI⁸, J. DUNLOP⁹, A. GALAMETZ¹, M. GIAVALISCO¹⁰, E. GIALONGO¹, A. KOEKEMOER¹¹,
R. MCLURE⁹, R. MAIOLINO¹², D. PARIS¹, AND P. SANTINI¹

¹ INAF Osservatorio Astronomico di Roma, Via Frascati 33, I-00040 Monteporzio (RM), Italy

² INAF Osservatorio Astronomico di Bologna, Italy

³ Department of Physics, University of California, Santa Barbara, CA 93106-9530, USA

⁴ Scuola Normale Superiore, Piazza dei Cavalieri 7, I-56126 Pisa, Italy

⁵ Max-Planck-Institut für Astrophysik, Karl-Schwarzschild-Str. 1, D-85741 Garching, Germany

⁶ Department of Physics, University of California, Davis, CA 95616, USA

⁷ School of Physics & Astronomy, University of Nottingham, Nottingham NG7 2RD, UK

⁸ INAF Osservatorio Astronomico di Trieste, Via G.B. Tiepolo 11, I-34131 Trieste, Italy

⁹ Institute for Astronomy, University of Edinburgh, Royal Observatory, Edinburgh EH9 3HJ, UK

¹⁰ Department of Astronomy, University of Massachusetts, Amherst, MA 01003, USA

¹¹ Space Telescope Science Institute, 3700 San Martin Drive, Baltimore, MD 21218, USA

¹² Kavli Institute for Cosmology, University of Cambridge, Madingley Road, Cambridge, CB3 0HA, UK

Received 2014 March 31; accepted 2014 July 15; published 2014 September 15

ABSTRACT

We present new results from our search for $z \sim 7$ galaxies from deep spectroscopic observations of candidate z dropouts in the CANDELS fields. Despite the extremely low flux limits achieved by our sensitive observations, only two galaxies have robust redshift identifications, one from its Ly α emission line at $z = 6.65$, the other from its Lyman break, i.e., the continuum discontinuity at the Ly α wavelength consistent with a redshift of 6.42 but with no emission line. In addition, for 23 galaxies we present deep limits in the Ly α equivalent width derived from the nondetections in ultradeep observations. Using this new data as well as previous samples, we assemble a total of 68 candidate $z \sim 7$ galaxies with deep spectroscopic observations, of which 12 have a line detection. With this much enlarged sample we can place solid constraints on the declining fraction of Ly α emission in $z \sim 7$ Lyman-break galaxies compared to $z \sim 6$, both for bright and faint galaxies. Applying a simple analytical model, we show that the present data favor a patchy reionization process rather than a smooth one.

Key words: galaxies: distances and redshifts – galaxies: formation – galaxies: high-redshift

Online-only material: color figures

1. INTRODUCTION

The use of Ly α transmission by the intergalactic medium (IGM) as a probe of its ionization state during the reionization epoch was proposed many years ago (Miralda-Escudé & Rees 1998; Santos et al. 2004). Strong Ly α emission powered by star formation is present in many distant galaxies: being a resonant line, it is sensitive to even small quantities of neutral hydrogen in the IGM, and it is easily suppressed (Loeb & Rybicki 1999; Malhotra & Rhoads 2006; Zheng et al. 2010). We thus expect the observed properties of Ly α -emitting galaxies to change at higher redshifts, when the IGM becomes more neutral. A very common approach for studying the reionization history of the universe using Ly α -emitting galaxies is to determine the evolution of the Ly α luminosity function and the clustering properties of narrow band selected Ly α emitters (LAEs; e.g., Ota et al. 2008; Ouchi et al. 2010; Kashikawa et al. 2011; Clément et al. 2012; Faisst et al. 2014). A recent complementary approach, the one used in this paper, is instead to measure the redshift evolution of the Ly α fraction in Lyman-break galaxies (LBGs), i.e., the percentage of LBGs that have an appreciable Ly α emission line (e.g., Stark et al. 2010). Indeed, this fraction is supposed to increase as we move to higher redshift because galaxies are increasingly young (hence with stronger intrinsic Ly α) and almost dust-free (Finkelstein et al. 2012), which facilitates the escape of Ly α photons. On the other hand, this fraction is expected to fall off as we approach the time when

the IGM becomes significantly neutral and the galaxies Ly α emission is progressively attenuated. Compared to other probes of reionization, such as the evolution of the LAE luminosity function, this approach can overcome concerns about intrinsic density evolution of the underlying population (Stark et al. 2010).

Intriguingly, early measurements with this technique suggest a strong drop in the Ly α fraction near $z \sim 7$, more significant for relatively fainter galaxies. In particular, in a series of recent works, a lack of Ly α emission was found at $z \sim 7$ compared to $z \sim 6$ by several independent teams: in our previous observations (Pentericci et al. 2011; Vanzella et al. 2011; Fontana et al. 2010; P11, V11, and F10 from here on) we found four Ly α -emitting galaxies (plus another object with a tentative line detection) out of a sample of 20 robust candidates. Similar or lower fractions were found by Schenker et al. (2012), Caruana et al. (2012), Bradač et al. (2012), and Ono et al. (2012) although considerable field-to-field variations are present due to the small number of candidates observed in each sample (see for example Figure 8 in Ono et al. 2012). In our favored interpretation, the lack of line emission is due to a substantial increase in the neutral hydrogen content of the universe in the time between $z \sim 6$ and $z \sim 7$. Comparing our data to the predictions of the semianalytical models by Dijkstra et al. (2011), we concluded that to explain the observations a substantial change of the neutral hydrogen fraction of the order of $\Delta\chi_{\text{HI}} \sim 0.6$ in a time $\Delta z \sim 1$ was required, assuming that the

galaxies' physical properties remain constant during this time. Recent observations pushing to $z \sim 8$ are consistent with this interpretation (Treu et al. 2013; Schmidt et al. 2014).

However, other factors could also play a role in the Ly α quenching. In particular, we cannot rule out the possibility that a change in some of the intrinsic galaxy properties (the Lyman continuum escape fraction, wind properties, and dust content) could at least partially contribute to the lack of Ly α emission. Indeed, the interpretation of the results as only being due to the change in the neutral hydrogen fraction was questioned by several successive works (e.g., Jensen et al. 2013b; Forero-Romero et al. 2012; Bolton & Haehnelt 2013; Taylor & Lidz 2014; Dijkstra et al. 2014). In particular, Bolton & Haehnelt (2013) suggested that the opacity of the intervening IGM redward of rest-frame Ly α can rise rapidly in average regions of the universe simply because of the increasing incidence of absorption systems, which are optically thick to Lyman continuum photons. They claimed that the data do not require a large change in the IGM neutral fraction from $z \sim 6$ to ~ 7 . However, such a rapid evolution of the photoionizing background could be very difficult to achieve without requiring either a late reionization or an emissivity at $z < 6$, which is too high to be consistent with observations of the Ly α forest (e.g., Sobacchi & Mesinger 2014). Preliminary estimates suggest that the neutral fraction constraint relaxes only mildly when taking into account the absorption systems (Mesinger et al. 2014).

We also mention the very recent work by Taylor & Lidz (2014), pointing out that sample variance is not negligible for existing surveys. Considering the large spatial fluctuations of the medium owing to an inhomogeneous reionization, the required neutral fraction at $z \sim 7$ can somehow be reduced to less extreme values. Indeed, the observational results are presently based on small data sets, with considerable field-to-field variations (Pentericci et al. 2011) and mostly focusing on the brightest candidates ($M_{UV} < -20.5$).

The complex topology of reionization is also a highly debated matter. Depending on the nature of the main sources of reionization, it is expected that the characteristic scale of the reionization process might change substantially (Iliev et al. 2006; Furlanetto et al. 2006). Accurate theoretical predictions for the morphology and sizes of H II regions depend on the abundance and clustering of the ionizing sources themselves in addition to the underlying inhomogeneous density field and clumpiness of the gas in the IGM (McQuinn et al. 2007; Sobacchi & Mesinger 2014). Observations of Ly α -emitting galaxies and their clustering have the potential to reveal the signature of patchy reionization, although early results have been inconclusive (Kashikawa et al. 2011; Ouchi et al. 2010)

In this paper we present new observations of $z \sim 7$ candidates, significantly increasing the statistics of previous works (especially in the faint regime, thanks to the inclusion of lensed candidates), which will allow us to assess the emergence of Ly α emission at high redshift with greater accuracy and address some of the above issues. In Section 2 we present the new observations and the previous data available; in Section 3 we describe the simulations used to accurately evaluate the sensitivity of our spectroscopic observations. In Section 4 we first evaluate the new limits on the Ly α fractions at high redshift, and we derive the neutral hydrogen fraction that is needed to explain the observed decrease; then applying a simple phenomenological model we derive new constraints on the topology of reionization. In Section 5 we summarize our findings.

All magnitudes are in the AB system, and we adopt $H_0 = 70 \text{ km s}^{-1} \text{ Mpc}^{-1}$, $\Omega_M = 0.3$, and $\Omega_\Lambda = 0.7$.

2. OBSERVATIONS

In this section we summarize the new observations presented in this work as well as previous data that we will use in this paper.

2.1. UDS Field

We selected candidate $z \sim 7$ galaxies in the UDS field from CANDELS multiwavelength observations (Galametz et al. 2013). Objects were detected in the J band, and then the color selection criteria presented by Grazian et al. (2012) were applied.¹³ Observations were taken in service mode with the FORS2 spectrograph on the ESO Very Large Telescope (VLT). We used the 600Z holographic grating, which provides the highest sensitivity in the range 8000–10,000 Å with a spectral resolution of $R \simeq 1390$ and a sampling of 1.6 Å per pixel for a 1" slit. Out of the entire sample of z -dropout candidates (which consists of 50 galaxies), we placed a total of 12 galaxies in the slits (the selection was just driven by the geometry of the mask). The rest of the mask was filled with i dropouts (E. Vanzella et al., in preparation) and other targets such as massive high-redshift galaxies and active galactic nucleus candidates. The sources have been observed through slitlets 1" wide by 10"–12" long. The observation strategy was identical to the one adopted in P11 and previous papers: series of spectra were taken at two different positions, offset by 4" (16 pixels) in the direction perpendicular to the dispersion. The total net integration time was 15.5 hr for each object. Data were reduced using our dedicated pipeline, which was described in detail in F10 and V11. Here we only mention that our pipeline performs the sky subtraction as typically done for the near-IR, subtracting the sky background between two consecutive exposures, exploiting the fact that the target spectrum is offset due to dithering in the classic ABBA pattern. Our algorithm implements a AB sky subtraction joined with a zero (e.g., median) or first-order fit of the sky along columns that regularized possible local differences in the sky counts among the partial frames before they are combined. We find that this procedure ensures the best final results when searching for faint emission lines, especially in the reddest part of the spectra where many strong skylines are present. The two-dimensional sky-subtracted partial frames are also combined (in the pixel domain) to produce the weighted rms map associated with the final reduced spectrum. This allows us to calculate the two-dimensional signal-to-noise (S/N) spectra, useful to assess the reliability of the spectral features. Finally, we also take extra care in the alignment of the different frames before the combination.

For one of the candidates with a relatively bright continuum magnitude ($J = 25.98$), UDS29249, we detect a faint continuum emission in the red part of the spectrum beyond ~ 9100 Å as shown in Figure 1. The total integrated S/N of the flux is ~ 10 ; while the detection is relatively secure in the wavelength range 9160–9240 Å, the exact position of the break (that is ascribed to the IGM) is difficult to locate both because of the faintness of the emission and also because of the residuals of the bright-sky emission lines in the region immediately below 9100 Å. We conservatively estimate a redshift that ranges

¹³ Note that these observations were performed before the official CANDELS catalog was released. Therefore at the time of mask preparation we adopted the J -detected catalog already used in Grazian et al. and in other works.

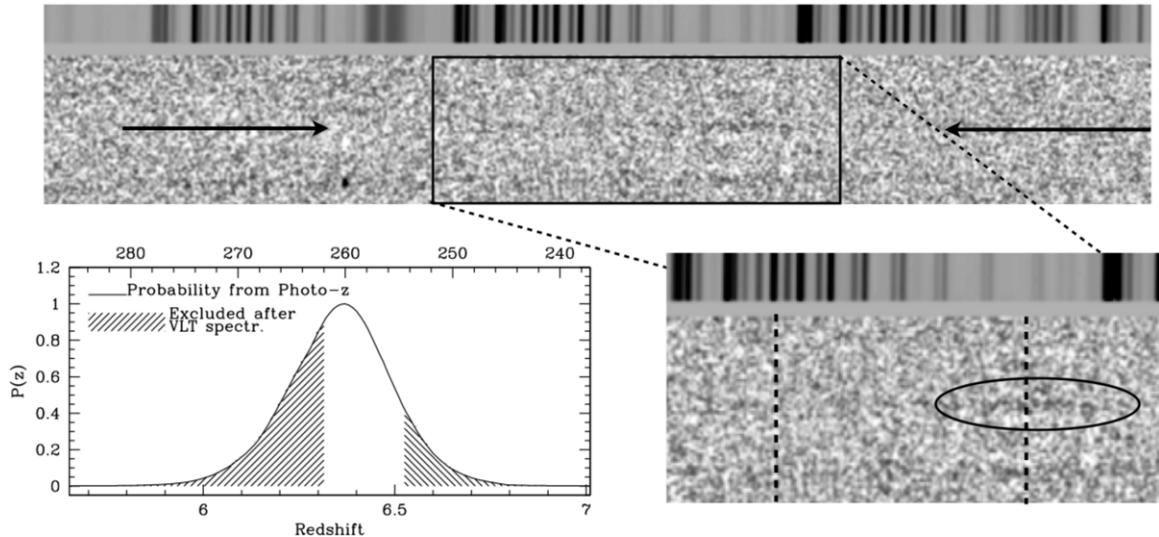


Figure 1. Upper panel shows the two-dimensional spectrum of galaxy UDS29249. The lower-right panel is an enlarged view of the wavelength range where we detect a faint continuum with an integrated S/N ~ 10 . The lower-left panel shows the probability distribution function of the photometric redshift obtained from the CANDELS photometry, which is further restricted when combined with the spectroscopic observations. In the upper panel note the presence of a serendipitous emission line to the lower left, coming from a redshift 6.058 galaxy.

between 6.31 and 6.53 (in the table we report 6.42 ± 0.11). Note that this is perfectly consistent with the photometric redshift distribution obtained from the CANDELS photometry, also shown in Figure 1. Recently Wilkins et al. (2014) discussed the possibility that a newly identified Y-dwarf population, as well as the late T-dwarf stars, might contaminate the photometric selection and spectroscopic follow-up of faint and distant galaxies (see also Bowler et al. 2014). Our target appears very compact but still resolved in the *Hubble Space Telescope* (HST) *J* band (as the majority of the $z \sim 7$ candidates); in addition its colors are not consistent with those of Y and T dwarfs. If we place the target in the $z - Y$ versus $Y - H$ plot, as in Figure 3 of Wilkins et al., the object is almost coincident with the high- z star-forming galaxy track and very distant from the position of both the L- and T-dwarf spectral standards as well as the tracks of the model Y dwarfs. Thus this gives us extra confidence that this is a true high-redshift galaxy without Ly α emission in its spectrum.

All other candidates are undetected (meaning that no feature is detected). In Table 1 we report the candidates, R.A. and decl., their *J*-band magnitudes, and the limiting equivalent width (EW). For the undetected objects we assume a redshift of 6.9, which is the median redshift of the selection function (see Grazian et al. 2012).

2.2. ESO Archive

We searched the ESO archive for observations of high-redshift objects; in particular we retrieved the data from the observations carried out within the program ESO 088.A-1013 (PI Bunker). This program used the same observational setup used above, with a total net integration time of 27 hr. It observed a mixture of z and *i* dropouts. Recently the results were presented by Caruana et al. (2014), and the authors report only one tentative detection at $z = 6.64$.

Caruana et al. have observed candidate high-redshift galaxies selected in previous works (Bouwens et al. 2011; McLure et al. 2010; Wilkins et al. 2011), which each used a different selection criteria, from different color-color cuts to photometric redshifts. Because we want to work on a sample that is as homogeneously

selected as possible, we have selected our own list of z dropouts, again using the color criteria presented by Grazian et al. (2012). We then cross-correlated our list with the targets in Caruana et al. (2014). We found nine matching objects, of which five are in common with the sample already observed in F10. We then retrieved the raw (public) data from the ESO archive and then processed through our own pipeline (V11) as all other data in this work. Here we present the results for the four new targets that are not in common with F10 (see Table 1). Further results, in particular the extremely deep combined spectra of the objects in common between the Caruana et al. program and F10 (52 hr), will be presented elsewhere (E. Vanzella et al., in preparation).

The results are again presented in Table 1. We detect a significant emission line in one of the four new objects, galaxy no. 34271 in the GOODS-Southfield corresponding to galaxy ERSz-2225141173 in Caruana et al. (2014). The line is detected at 9301 \AA and shows the typical asymmetry of Ly α , which would place the object at redshift 6.649 ± 0.001 . In Figure 2 we show the one-dimensional and two-dimensional spectra of the galaxy. The EW of the line is 43 \AA , calculated from its measured line flux and the *Y*-band magnitude from the GOODS CANDELS catalog.

Caruana et al. (2014) report only a tentative ($<5\sigma$) detection for this object. We ascribe the difference to the fact that for most of the data-reduction steps the authors used the standard ESO pipeline, while we use our own pipeline that has been tailored specifically to the detection of faint high-redshift emission lines (see the description above). The other three targets are undetected, and we can set stringent limits on their Ly α EW limit, ranging from $\sim 10 \text{ \AA}$ to $\sim 25 \text{ \AA}$ depending on the continuum magnitude and assuming that they are placed at redshift 6.9. Obviously the actual EW limit depends sensibly on the exact redshift of the objects (see F10 Figure 1).

2.3. Data from Previous Literature

Besides the new data, we include all previously published spectroscopic data on z dropouts in order to assemble the largest possible sample of candidate $z \sim 7$ galaxies with deep spectroscopic observations.

Table 1
Spectroscopic Properties of Observed z Dropouts in the New Fields

UDS							
ID	R.A.	Decl.	J125		M_{UV}	z	EW(S/N = 5)
29249	34.226135	5.1510921	25.985		-20.93	$\sim 6.42 \pm 0.11$	<9
28737	34.229103	5.1533098	25.967		-20.95	...	<12
16910	34.226192	5.2033339	26.503		-20.42	...	<20
23427	34.298386	5.1760311	25.826		-21.09	...	<10
15399	34.233883	5.2100158	25.426		-21.49	...	<7
16119	34.253719	5.2068028	26.297		-20.62	...	<16
16669	34.279049	5.2043710	26.479		-20.44	...	<19
16974	34.313725	5.2030821	26.02		-20.87	...	<12
16094	34.3180048	-5.2069350	27.006		-19.91	...	<30
14435	34.323608	5.2141371	26.570		-20.35	...	<20
8912	34.2815881	-5.23757910	26.805		-20.11	...	<25
12402	34.3203425	-5.22268940	27.013		-19.90	...	<30
GOODS-S							
ID	R.A.	Decl.	J125		M_{UV}	z	EW
20439	53.09556	-27.73609	27.11		-19.81	...	<25
24805	53.11627	-27.6845	26.08		-20.84	...	<10
14259	53.16164	-27.78533	27.08		-19.84	...	<25
34271	53.09377	-27.68814	27.44		-19.48	6.65	43
Bullet							
ID	R.A.	Decl.	J110	J110 intrinsic	M_{UV} intrinsic	z	EW
1	104.65470	55.974464	26.88	28.45	-18.52	...	<25
2	104.65527	55.971901	27.03	29.05	-17.92	...	<29
3	104.66736	55.968067	25.43	28.13	-18.84	...	<7
4	104.66375	55.928802	26.88	27.97	-19.00	...	<25
5	104.63437	55.978603	25.98	26.78	-20.19	...	<11
6	104.62446	55.951065	25.87	28.38	-18.59	...	<10
7	104.64304	55.964756	25.95	27.75	-19.22	...	<11
8	104.64549	55.924828	26.29	27.52	-19.45	...	<15
9	104.63254	55.963764	26.46	28.05	-18.92	...	<17
10	104.63015	55.970482	26.47	27.67	-19.30	6.740	30

In particular we consider the following: (1) The 20 z dropouts selected in the GOODS-South, NTTDF, and BDF4 fields (Castellano et al. 2010a, 2010b), whose observations were carried out by our groups in P11 and previously presented by V11 and F10. Of these, four show a convincing Ly α emission line, while the tentative detection of a fifth candidate originally shown in F10 was not confirmed by the combination of our own data with the deeper observations of Caruana et al. (2014; E. Vanzella et al., in preparation). (2) The 11 bright z dropouts observed by Ono et al. (2012) in the SDF field, of which three have bright Ly α in emission. These candidates were detected in deep Y -band observations and selected using color criteria that are very similar to ours. (3) A subset of the objects presented by Schenker et al. (2012). In particular, we select those galaxies whose colors are consistent with the z -dropout selection criteria used in this paper (note that Schenker et al. also observed Y -band dropouts whose photometric redshifts are $\gg 7$). In total we consider 11 objects, of which two are detected with Ly α .

Overall, considering new and previous data, we assemble a sample of 68 z dropouts that have been spectroscopically observed with either VLT, Keck, or Subaru down to very faint flux limits. Note that 46 out of 68 have been observed with exactly the same setup (with FORS2@VLT using grism 600 z).

2.4. Bullet Cluster

Bradač et al. (2012) observed the lensed z dropouts detected behind the Bullet cluster and selected by Hall et al. (2012).

The observations were carried out with FORS2@VLT using the same observational setup as in our various programs (V11, P11) and above (UDS and GOODS-S) with a total net integration time of 16.5 hr. Data were reduced using our own pipeline (V11).

The confirmation of one galaxy showing Ly α emission consistent with a redshift of 6.74 was presented by Bradač et al. (2012). Here we also consider the observations and limits in terms of Ly α line detection of the rest of the sample. In Table 1 we report the resulting limits on the Ly α EW for each galaxy, assuming again a median redshift of 6.9. However, note that in this case the median expected redshift of the sample is > 7 : the redshift probability distribution function of these candidates is much larger and extends well beyond $z = 8$, differing considerably from the other samples presented here (for reference see Figure 5 in Hall et al. 2012). This is because the candidates were selected by applying criteria based on a $z_{850} - J_{110}$ color (due to the nature of the *HST* data available). In the following section we will consider, whenever necessary, the appropriate selection function of this sample.

3. SIMULATIONS

To determine the EW limit achieved by our observations for each of our targets and reported in Table 1, we performed detailed two-dimensional simulations that we briefly describe here. We take real individual MXU raw frames corresponding to slits where no targets were detected and insert an emission line of a given flux, at a given wavelength, and at a given spatial

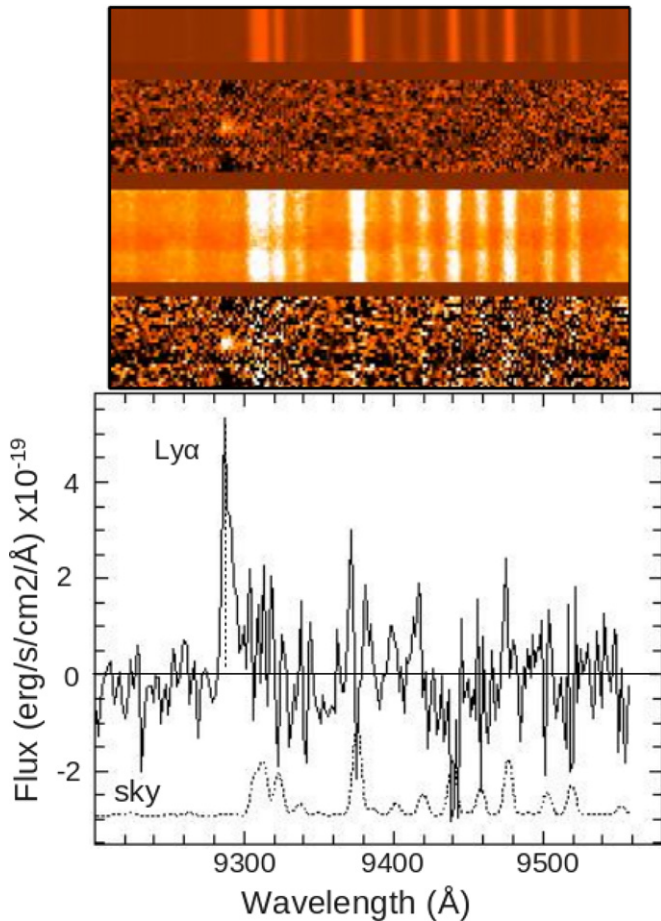


Figure 2. Upper panels show the two-dimensional spectrum of the galaxy GDS34271 (ERSz-2225141173 in Caruana et al. 2014) showing the Ly α line at 9300 Å. From top to bottom the panels represent the sky emission, the S/N spectrum, the total rms, and the reduced spectrum. The bottom panel is the one-dimensional extracted spectrum after smoothing by two pixels.

(A color version of this figure is available in the online journal.)

position corresponding to the middle of the slit. The emission line is modeled as a Gaussian that is then truncated to half to simulate the typically asymmetric emission lines that are routinely observed at lower redshift and then further convolved with the seeing (with values varying from 0.6 to 1.2 as in the real observations). The individual frames are then processed as normally done during the reduction procedure: after standard flat-fielding, we remove the sky emission lines by subtracting the sky background between two consecutive exposures, exploiting the fact that the target spectrum is offset due to dithering (ABBA technique). Then spectra are wavelength-calibrated (using lamp exposures), and finally they are flux-calibrated using the observations of spectrophotometric standards and combined.

The resulting two-dimensional frame is then scanned with a window of 7×5 pixels to see if there is a detection, and in this case the S/N of the line is registered. The simulations are repeated after shifting the Ly α emission line along the dispersion axis in steps of 1.6 Å, and in the end we cover the redshift range from $z = 5.68$ to $z = 7.30$. At each redshift step, the scan is repeated and the S/N of the line is registered again.

The emission lines are then varied in terms of total flux (from 0.24 to 1.6×10^{-17} erg s $^{-1}$ cm $^{-2}$) and full width at half-maximum (FWHM; varying from 230 to 520 km s $^{-1}$). These values are in the range of the real observed Ly α lines. The entire procedure is repeated for each combination of line flux

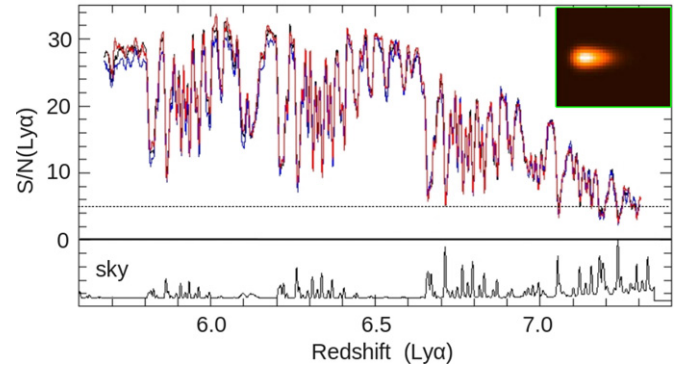


Figure 3. Results from our two-dimensional simulations. The colored curves represent the S/N corresponding to a line with flux $1.6e \times 10^{-17}$ erg s $^{-1}$ cm $^{-2}$ and FWHM = 300 km s $^{-1}$ at each different redshift. Each of the colors corresponds to simulations performed using a different slit in the two chips. For each slit the curves are the average of the S/N obtained at five different positions, respectively -10 , -5 , 0 , $+5$, and $+10$ pixels along the positional axis with respect to the center of the slit. In the inset at the top-right corner of the figure we show a simulated Ly α line that is inserted in the raw frames for these simulations. In the lower panel we show the skyline emission.

(A color version of this figure is available in the online journal.)

and FWHM. The simulations were performed for more than one slit in order to cover the entire CCD (top and bottom chips) of the FORS2 MXU frame, and the results are always the same to within 5%. Although our candidates were placed at the center of the slits in most cases, we also checked for possible differences by placing the initial emission line at various positions along individual slits, i.e., we shifted the Ly α up and down by a few pixels. Again no significant difference was found. In Figure 3 we show one of the results of these tests, with the three colored curves (red, green, and black) representing the resulting S/N of a line with flux $1.6 \sim 10^{-17}$ erg s $^{-1}$ cm $^{-2}$, positioned in three different slits: for each slit the result is the average of three different positions along the spatial axis (0, +5, and -5 pixel). It is evident that the differences in the resulting S/N between slits are only marginal. In the same figure we also show the skyline emission for reference.

4. THE DECLINING FRACTION OF LAEs: NEW LIMITS AND DISCUSSION

4.1. The Fraction of LAEs at $z \sim 7$

With our new sample we can evaluate with greater accuracy the fraction of Ly α emission in LBGs at redshift 7, the decline between $z \sim 6$ and $z \sim 7$, and its implications. In Table 2 we report the fraction of galaxies having an EW > 25 Å and > 50 Å separately for the two absolute-magnitude bins that were adopted by previous works (Stark et al. 2010; P11; Ono et al. 2012). In the bright bin (galaxies with magnitudes $-21.25 < M_{UV} < -20.25$) there are 39 galaxies, of which seven are detected in Ly α : five of these have EW > 25 Å two have EW > 50 Å and none has EW > 75 Å. In the faint bin (galaxies with $-20.25 < M_{UV} < -18.75$) there are 25 objects, of which five have a Ly α emission with EW > 25 Å and two with EW > 50 Å. Note that three of the targets in the Bradač et al. sample are intrinsically fainter than $M_{UV} = -18.75$ and thus are excluded from this bin. In the table we report the fractions taking into account the fact that the limit in the EW detectable for the galaxies is not always below 25 Å; for example, for some of the objects in Ono et al. (2012) the limits achieved are above this value. In calculating the fractions, we also consider

Table 2
Fractions of Ly α Emission

Mag	Interlopers	EW > 25 Å	EW > 50 Å	EW > 75 Å
$-21.25 < M_{UV} < -20.25$	None	$0.15^{+0.11}_{-0.08}$	$0.06^{+0.07}_{-0.04}$	<0.05
	20%	$0.19^{+0.13}_{-0.10}$	$0.07^{+0.09}_{-0.05}$	<0.06
$-20.25 < M_{UV} < -18.75$	None	$0.29^{+0.20}_{-0.15}$	$0.10^{+0.13}_{-0.06}$	<0.08
	20%	$0.36^{+0.25}_{-0.18}$	$0.12^{+0.17}_{-0.08}$	<0.10
All	None	$0.19^{+0.08}_{-0.06}$	$0.07^{+0.05}_{-0.03}$	<0.031
	20%	$0.23^{+0.10}_{-0.07}$	$0.09^{+0.07}_{-0.04}$	<0.039

Note: The limits at 75 Å have been calculated using the confidence limits for small numbers of events (Gehrels 1986). Note that the bin with all galaxies also contains few objects that are fainter than the -18.75 limit.

that for some galaxies the redshift probability distribution extends well beyond $z \sim 7.3$, which is approximately the limit out to which we can detect the Ly α emission in our current observations. In particular as already stated above, the sample observed by Bradač et al. (2012) was selected in such a way that the probability of galaxies being at $z > 7.3$ is quite high, $\sim 48\%$ (see Figure 5 in Hall et al. 2012). This is due to the broad J -band filter ($J110$) that was available for the selection. Therefore we weighted each sample by evaluating the total probability of galaxies being outside the redshift range that is observable by the spectroscopic setup. In practice for most of the samples this probability is negligible (see Figure 6 in Ouchi et al. 2010 for the Ono et al. sample, Figure 7 in Castellano et al. 2010a for the NTT, GOODS-South, and BDF samples), while it is non-negligible for the UDS sample (which has a tail to $z \sim 8$; see Figure 1 in Grazian et al. 2012) and quite high for the Bradač et al. sample.

We also report the fractions after assuming that 20% of the undetected objects are lower redshift interlopers: this value (20%) is the upper limit for possible interlopers found in a large sample of $z \sim 6$ galaxies in our previous work (P11), and we assume that there is no significant change between the two epochs. Note that none of our galaxies has a detected Ly α emission with EW larger than 75 Å: to calculate the upper limit for the fraction, we assume the statistics for small numbers of events by Gehrels (1986).

Comparing the above results to those at $z \sim 6$ presented by Stark et al. (2010), it is clear that there is a very significant deficit of Ly α emission at $z \sim 7$ compared to earlier epochs. We note here that very recently Schenker et al. (2014) introduced a new method to analyze the decrease of Ly α emission in LBGs, based on using the measured slopes of the rest-frame ultraviolet continua of galaxies rather than their absolute M_{UV} magnitudes as we do here. According to their conclusions, the observed difference between the $z \sim 6$ and $z \sim 7$ EW distributions is even slightly larger than with the traditional way of computing fractions in bins of M_{UV} . This is mainly because blue galaxies at $z \sim 6$ exhibit stronger Ly α emission and candidates at $z \sim 7$ tend to be bluer than at lower redshift; hence they are expected to exhibit Ly α even more often.

In the following sections we will try to interpret this deficit, first within the context of large-scale seminumeric simulations of reionization that include the reionization field as well as galactic properties (Dijkstra et al. 2011). We will then apply to our data a simple phenomenological model developed by Treu et al. (2012) that uses the evolution of the distribution of Ly α EWs to make some simple predictions about the complex topology of reionization.

4.2. The Neutral Hydrogen Fraction

In P11 we interpreted the drop in the Ly α fraction in LBGs as due most probably to the sudden increase of neutral hydrogen in the universe between $z \sim 6$ and $z \sim 7$ (see also Schenker et al. 2012). We then compared the results to the predictions of Dijkstra et al. (2011) to determine what fraction of neutral hydrogen would be needed to explain the drop, provided that all other physical parameters (e.g., dust content and the escape fraction of Lyman continuum photons) would not change between $z = 6$ and $z = 7$. We obtained a rather high neutral hydrogen fraction by volume, $\chi_{H1} \sim 0.6$.

We now make use of improved models to compare our new results. As in Dijkstra et al. (2011), reionization morphologies were generated using the public code DexM (Mesinger & Furlanetto 2007). The box size is 200 Mpc, and the ionization field is computed on a 500^3 grid. Reionization morphologies at a given χ_{H1} are generated by varying the ionization efficiency of halos, down to a minimum halo mass of $5 \times 10^8 M_{\odot}$, roughly corresponding to the average minimum mass of halos at $z = 7$ that retain enough gas to form stars efficiently (Sobacchi & Mesinger 2013). Compared to P11, the model now also includes more massive halos with stellar masses up to $10^{12} M_{\odot}$. This is because the previous model was tailored to analyze the nature of fainter dropout galaxies (Dijkstra et al. 2011) compared to those presented in this work. The results however change only minimally with the new choice of halo mass, as expected given that the halo bias (and the associated opacity distribution for a given χ_{H1}) does not evolve much over this mass range (e.g., Mesinger & Furlanetto 2008; McQuinn et al. 2008). In Figure 4 we present the comparison of the outcome of the new model with the present fractions for the faint sample. The red circles (and limit) show the fractions assuming that all of our nondetected targets are at $z \sim 7$ (the same assumption that is made in this model at $z \sim 6$), while the blue circles and limit assume 20% interlopers. It is clear that only a very high neutral hydrogen fraction ($\chi_{H1} \geq 0.51$) can best reproduce the lack of Ly α emission at $z = 7$ compared to earlier epochs, even if there are still considerable uncertainties, i.e., large error bars due to the small size of the samples. This high value seems at odds with other observational results: for instance, Raskutti et al. (2012) study the IGM temperature in quasar near-zones and find that reionization must have been completed by $z > 6.5$ at high confidence, while several teams (Hu et al. 2010; Kashikawa et al. 2011; Ouchi et al. 2010) study the Ly α line shapes of LAEs at $z = 6.5$, finding no evidence of damping wings.

As recently pointed out by Taylor & Lidz (2014), before reionization completes, the simulated Ly α fraction might have large

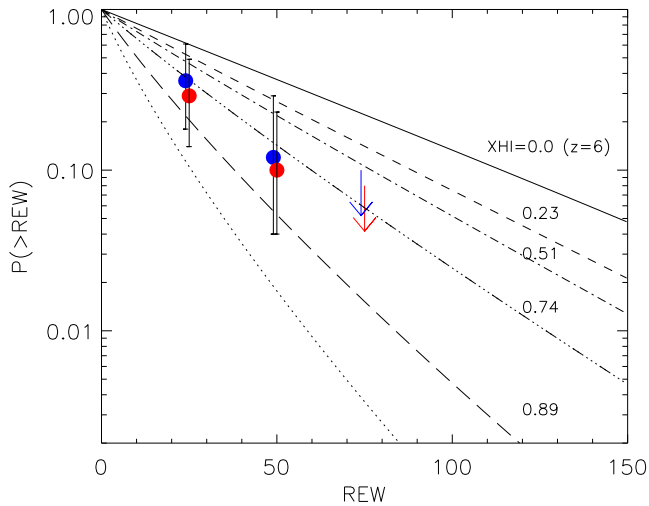


Figure 4. Expected cumulative distribution of Ly α detections as a function of rest-frame EWs for $z \sim 7$ faint LBGs, under the assumption that the observed LAE fraction at $z \sim 7$ is different from $z \sim 6$ only because of the IGM. The different lines correspond to a universe that was respectively $\sim 0.0, 0.23, 0.51, 0.74, 0.89$ neutral by volume (from top to bottom) at $z = 7$. The line for $\chi_{\text{HI}} = 0.0$ is the same as at $z = 6$. The lines correspond to the model with $N_{\text{HI}} = 10^{20} \text{ cm}^{-2}$ and $v_{\text{wind}} = 200 \text{ km s}^{-1}$. The red (blue) circles and limits are our results assuming that 0 (20)% of the undetected galaxies are interlopers, respectively (from Table 2).

(A color version of this figure is available in the online journal.)

spatial fluctuations depending on the degree of homogeneity/inhomogeneity of the reionization process. Because existing measurements of the Ly α fraction span relatively small regions on the sky and sample these regions only sparsely (typically only a few dropouts are observed per field), they might by chance probe mostly galaxies with above-average Ly α attenuation and therefore point to higher neutral hydrogen fractions compared to the average values. It is therefore important to include the effect of cosmic variance for different sight lines within our survey. In their work, Taylor & Lidz found that the sample variance is non-negligible for existing surveys, and it does somewhat mitigate the required neutral fraction at $z \sim 7$.

Compared to previous studies and to the surveys analyzed by Taylor & Lidz, this work presents more independent fields of view: even considering as single pointing those in adjacent areas (e.g., the GOODS-South/ERS areas and the two SDF pointings in Ono et al. 2012), we are now sampling eight independent lines of sight, with areas varying between 50–100 arcmin² in each field. We have verified what is the uncertainty in our results that might be derived from the cosmic variance.

We have tried to quantify what is the variance in the opacity ($e^{-\tau_{\text{reion}}}$) in the simulations due to the limited number of fields analyzed. In the simulations we take eight random regions with areas corresponding to our observed fields, and in each field we sample a reasonable number of lines of sight (corresponding to the average number of candidates spectroscopically observed). We then compute the pointing-to-pointing (cosmic) standard deviation $\sigma_{\text{FOV}}(e^{-\tau})$, which for eight fields is on the order of 6%. The variance is so small because the total volume sampled is quite large. We also varied the number of candidate galaxies probing the reionization per each pointing: indeed the discreteness in sampling the reionization morphology becomes an issue, especially for large neutral fractions because in this case the lesser number of would-be LAEs can miss the relatively rare regions in a given pointing that have a high transmission. However, even considering a small sampling (only five emitters

per pointing), $\sigma_{\text{FOV}}(e^{-\tau})$ is still around 10%. Note that this computation just uses the opacity at a single wavelength, roughly 200 km s^{-1} redward of the line center, where most of the intrinsic emission is expected to lie. This is not really the variance in the Ly α fraction because the latter requires some more detailed modeling, but it gives a crude idea of what is the expected cosmic variance from reionization. Therefore we are quite confident that for our sample, which has a large number of independent fields and a reasonable number of candidates observed per pointing, the field-to-field fluctuations are not very large and would not affect sensibly the results of Figure 4.

4.3. A Patchy Reionization Process?

Applying the simple phenomenological models developed by Treu et al. (2012) to describe the evolution of the distribution of Ly α EWs, we can now use the Ly α detections and nondetections to make some inferences about the complex topology of reionization. This model starts from the intrinsic rest-frame distribution in terms of the one measured at $z \sim 6$ by Stark et al. (2011). It then considers two extreme cases that should bracket the range of possible scenarios for the reionization morphology: in the first (“patchy”) model, no Ly α is received from a fraction ϵ_p of the sources, while the rest are unaffected. In the second (“smooth”) model, the Ly α emission is attenuated in every galaxy in the same way, by a factor ϵ_s . These two models can be thought of respectively as simple idealizations of smooth and patchy reionization: although very simple and somewhat unphysical (especially the smooth one), these two models should bracket the expected behavior of the IGM near the epoch of reionization (see Treu et al. 2012 and Treu et al. 2013 for a more detailed explanation).

For each object in our sample, Bayes’ rule gives the posterior probability of ϵ_p and ϵ_s (which we collectively indicate as ϵ) and redshift given the observed spectrum and the continuum magnitude. The likelihood is as usual the probability of obtaining the data for any given value of the parameter. The model adopts a uniform prior $p(\epsilon)$ between zero and unity, while the prior for the redshift $p(z)$ is obtained from the redshift probability distribution (as described in Section 3 for each of the different parent samples). We use the implementation of the method that takes as input the line-EWs or EW limits, in order to incorporate all of the available information even when a noise spectrum is not available (Treu et al. 2012).

One of the outputs of the model is the normalization constant Z , known as the Bayesian evidence and which quantifies how well each of the two models matches the data. The evidence ratio is a powerful way to perform model selection, e.g., comparing the patchy and smooth models, and eventually discriminate between the two.

Treu et al. 2012 applied their model to the sample presented by Ono et al. (2012), which also included data from P11 and V11. The data clearly preferred an attenuation factor of $\epsilon < 1$ (0.65–0.68), independent of the model considered, but the evidence ratio indicated no significant preference for either of the two models.

We have repeated the exercise for our new enlarged sample, which is almost double compared to the previous one and most importantly contains a larger fraction of very faint galaxies, (thanks for example to the inclusion of the lensed galaxies of the Bradac et al. sample and several other faint targets from UDS and the archival data). With the new sample we obtain $\epsilon_p = 0.46 \pm 0.12$ and $\epsilon_s = 0.60 \pm 0.09$, respectively, for the patchy and smooth models, as shown in Figure 5: this

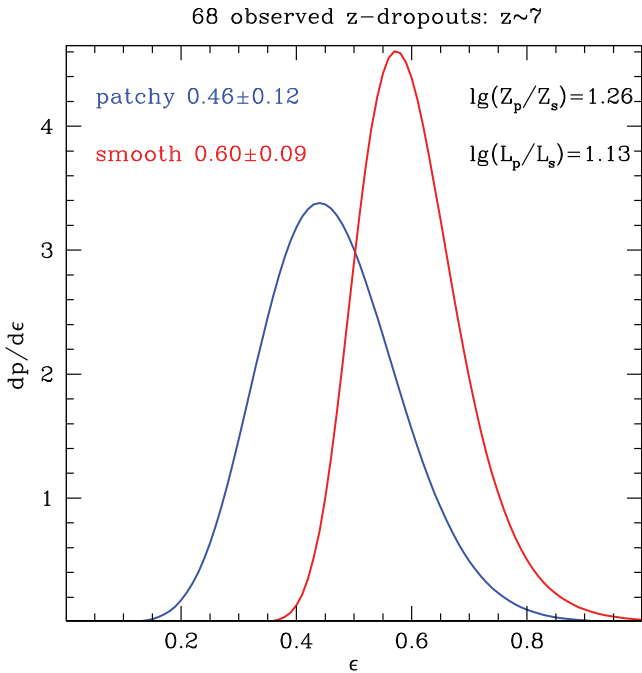


Figure 5. Marginalized posterior distribution function of ϵ at $z \sim 7$ based on a compilation of 68 z dropouts with deep spectroscopic follow-up presented in this paper or taken from the literature (Pentericci et al. 2011; Ono et al. 2012; Schenker et al. 2012). Both the patchy and smooth models indicate clearly that the Ly α emission is significantly quenched at $z \sim 7$ with respect to $z \sim 6$ (i.e., $\epsilon < 1$).

(A color version of this figure is available in the online journal.)

means that both models require a considerable quenching of the Ly α compared to $z \sim 6$, as expected from the many nondetections. Note that these results assume that the level of contamination in the samples is the same at $z = 6$ and at $z = 7$. We can interpret the ϵ_p and ϵ_s as the average excess optical depth of Ly α with respect to $z \sim 6$, i.e., $\langle e^{-\tau_{\text{Ly}\alpha}} \rangle$, although a conversion from this to a neutral hydrogen fraction requires detailed and uncertain modeling (e.g., Santos 2004). A key result is that with the new sample the evidence ratio between the two models is quite high, $\log(Z_p/Z_s) = 1.26$, which means that the patchy model is highly favored (>18 times) by the data over the smooth one. This is also suggested by the likelihood ratio test: L_p/L_s strongly favors the patchy model (in other terms, the ratio corresponds to a difference in $\Delta\chi^2$ between the two models of $2 \ln(L_p/L_s) \sim 5.2$). As expected, the power to discriminate between the two models is given by the inclusion of fainter galaxies as well as the fact that for many galaxies we have very deep EW limits. As a result of the inference, the model also allows us to calculate the fraction of emitters using all of the available information. For objects brighter than $M_{\text{UV}} = -20.25$ the model predicts, respectively, 0.09 ± 0.04 for galaxies with $\text{EW} > 25 \text{ \AA}$ and 0.03 ± 0.02 for galaxies with $\text{EW} > 55 \text{ \AA}$. For fainter galaxies, the predictions are 0.24 ± 0.08 and 0.12 ± 0.05 , respectively. These values are very close to the numbers reported in Table 2 (considering obviously the fractions derived assuming no interlopers in the sample). In Figure 6 we show the predicted distribution of rest-frame EW for the best patchy (blue) and smooth (red) models for the bright and faint subsamples separately. The black histograms are based on the detected LAEs in each sample. In particular, the blue model makes predictions that are closer to the real data for the faint subsample because it better predicts the high EW tail and it does not show a deficit of detections at intermediate EW

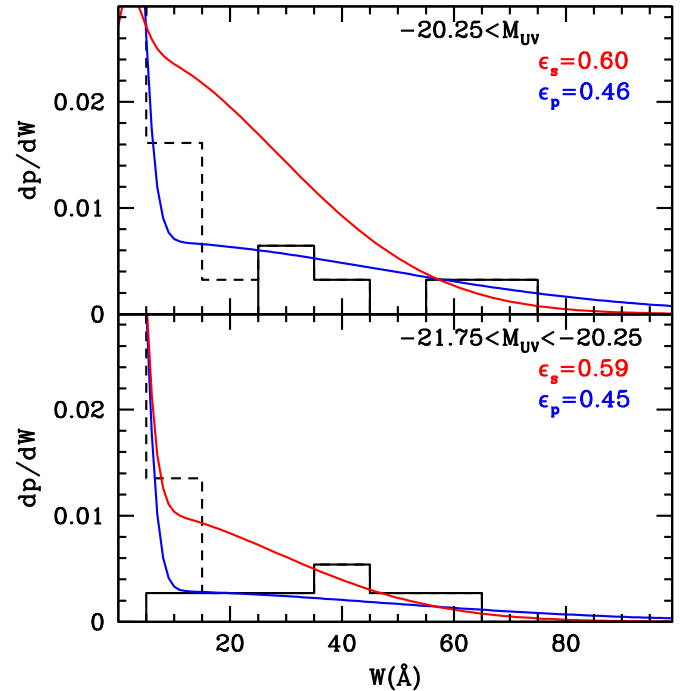


Figure 6. Predicted distribution of rest-frame equivalent width for the best patchy (blue) and smooth (red) models for the bright subsample (top panel) and faint subsamples (lower panel). The black histograms are based on the detected Ly α emitters in each sample, while the dashed ones assume that all undetected objects have a Ly α that is immediately below the threshold (so they represent upper limits).

(A color version of this figure is available in the online journal.)

($\sim 30\text{--}40 \text{ \AA}$). While our observational results indicate clearly that the distribution of neutral hydrogen in these phases of reionization was highly inhomogeneous, as expected by most theoretical predictions (e.g., Iliev et al. 2006), to fully constrain the morphology of reionization we will have to wait for the direct observations of the 21 cm emission from neutral hydrogen in the high-redshift universe, which is one of the prime tasks of the upcoming LOFAR survey observations (e.g., Jensen et al. 2013a).

5. SUMMARY AND CONCLUDING REMARKS

In this paper we have presented new results from our search for $z \sim 7$ galaxies from deep spectroscopic observations of candidate z dropouts in the CANDELS fields. Even though our sensitive VLT observations reached extremely low flux limits, only two galaxies have new robust redshift identifications, one from the Ly α emission line at $z = 6.65$ and the other from its Ly α break, i.e., the continuum discontinuity at the Ly α wavelength consistent with a redshift of ~ 6.42 . In this second object no emission line is observed. In addition, for 23 galaxies we present new deep limits on the Ly α EW derived from the nondetections in ultradeep observations (from 15 to 27 hr) obtained with the FORS2 spectrograph on the VLT. Using this new data as well as previously published samples, we have assembled a total of 68 candidate $z \sim 7$ galaxies with deep spectroscopic observations, of which 12 have a redshift identification from the Ly α emission line. With this much enlarged sample we have placed solid constraints on the fraction of Ly α emission in $z \sim 7$ LBGs for both bright and faint galaxies, confirming the large decline in the presence of Ly α emission from $z \sim 6$ to $z \sim 7$. If this decline is only due to the evolution of the IGM, and assuming that all other

galaxy properties remain unchanged in this redshift interval, a very large fraction ($\chi_{\text{HI}} \geq 0.51$) of neutral hydrogen is needed to explain the observations. Finally, applying the simple phenomenological model developed by Treu et al. (2012), we show that the present data favor a patchy reionization process rather than a smooth one, as expected from most simulations (e.g., Friedrich et al. 2011; Choudhury et al. 2009; Iliev et al. 2006, to name a few; also see Trac & Gnedin 2011 for a review on simulations of reionization).

Obviously we cannot rule out that an evolution of other properties, namely f_{esc} and dust, come into play and contribute to the Ly α quenching.¹⁴ Indeed, in a recent paper (Dijkstra et al. 2014) we discuss the possibility that the decline in strong Ly α emission from $z > 6$ galaxies is due, in part, also to an increase of the Lyman continuum escape fraction in star-forming galaxies. In particular, assuming that the escape fraction evolves with redshift as $f_{\text{esc}}(z) = f_0([1+z]/5)^k$ (as in Kuhlen & Faucher-Giguere 2012), and taking $k = 4$ and $f_0 = 0.04$ such that we have $f_{\text{esc}} = 0.15$ at $z = 6$ and $f_{\text{esc}} = 0.26$ at $z = 7$, the observed decline in Ly α emission could be reproduced with a more modest evolution in the global neutral fraction, on the order of $\Delta\chi_{\text{HI}} \sim 0.2$. This work is clearly rather speculative because f_{esc} is a very elusive quantity to measure and we only have tentative indications on its value from upper limits (e.g., Nestor et al. 2013; Vanzella et al. 2012; Boutsia et al. 2011) and on its evolution (e.g., Cowie et al. 2009; Siana et al. 2010). However, it shows that an evolving escape fraction of ionizing photons should be considered as part of the explanation for evolution in the Ly α emission of high-redshift galaxies in addition to the evolution of the IGM (see Dijkstra et al. 2014 for more details).

It is clear that to fully characterize and understand the reionization epoch and to clarify the relation between the disappearing Ly α emission line and cosmic reionization we still have to make a substantial effort on both the observational and modeling sides. Even if the current samples of candidate galaxies at $z > 7$ are quite large, and despite all the observational efforts by several teams, the number of spectroscopically confirmed objects remains very small. To overcome this limitation and substantially increase the statistics, we are currently carrying out an ESO Large Program with FORS2@VLT (PI Pentericci) that in the end should allow us to increase considerably the number of confirmed high-redshift galaxies by observing ~ 200 candidates. In particular, because the targets will be selected from the CANDELS field with extremely deep near-IR observations, we will also include galaxies as faint as $J = 27$. The new deep spectroscopic observations will allow us to assess the continuous evolution of the Ly α emission over the range $6 < z < 7.3$, and from a comparison to state-of-the-art models, we will be able to determine if the Ly α was mainly quenched by the neutral IGM or if any evolution of the galaxies' physical properties also played a significant role.

Part of this work has been funded through INAF Grants (PRIN-INAF 2010 and 2012). R.J.M. acknowledges the support of the European Research Council via the award of a Consolidator Grant. J.S.D. acknowledges the support of the European Research Council via the award of an Advanced Grant, the support

of the Royal Society via a Wolfson Research Merit Award, and the contribution of the EC FP7 SPACE project ASTRODEEP (Ref. No: 312725).

REFERENCES

- Bolton, J. S., & Haehnelt, M. G. 2013, *MNRAS*, 429, 1695
 Boutsia, K., Grazian, A., Giallongo, E., et al. 2011, *ApJ*, 736, 41
 Bouwens, R. J., Illingworth, G. D., Oesch, P. A., et al. 2011, *ApJ*, 737, 90
 Bowler, R. A. A., Dunlop, J. S., McLure, R. J., et al. 2014, *MNRAS*, 440, 2810
 Bradač, M., Vanzella, E., Hall, N., et al. 2012, *ApJL*, 755, L7
 Caruana, J., Bunker, A. J., Wilkins, S. M., et al. 2012, *MNRAS*, 427, 3055
 Caruana, J., Bunker, A. J., Wilkins, S. M., et al. 2014, *MNRAS*, 443, 2831
 Castellano, M., Fontana, A., Boutsia, K., et al. 2010a, *A&A*, 511, A20
 Castellano, M., Fontana, A., Paris, D., et al. 2010b, *A&A*, 524, A28
 Choudhury, T. R., Haehnelt, M. G., & Regan, J. 2009, *MNRAS*, 394, 960
 Clément, B., Cuby, J.-G., Courbin, F., et al. 2012, *A&A*, 538, A66
 Cowie, L. L., Barger, A. J., & Trouille, L. 2009, *ApJ*, 692, 1476
 Dijkstra, M., Mesinger, A., & Wyithe, J. S. B. 2011, *MNRAS*, 414, 2139
 Dijkstra, M., Wyithe, S., Haiman, Z., Mesinger, A., & Pentericci, L. 2014, *MNRAS*, 440, 3309
 Faist, A. L., Capak, P., Carollo, C. M., Scarlata, C., & Scoville, N. 2014, *ApJ*, 788, 87
 Finkelstein, S. L., Papovich, C., Salmon, B., et al. 2012, *ApJ*, 756, 164
 Fontana, A., Vanzella, E., Pentericci, L., et al. 2010, *ApJL*, 725, L205
 Forero-Romero, J. E., Yepes, G., Gottlöber, S., & Prada, F. 2012, *MNRAS*, 419, 952
 Friedrich, M. M., Mellema, G., Alvarez, M. A., Shapiro, P. R., & Iliev, I. T. 2011, *MNRAS*, 413, 1353
 Furlanetto, S. R., McQuinn, M., & Hernquist, L. 2006, *MNRAS*, 365, 115
 Galametz, A., Grazian, A., Fontana, A., et al. 2013, *ApJS*, 206, 10
 Gehrels, N. 1986, *ApJ*, 303, 336
 Grazian, A., Castellano, M., Fontana, A., et al. 2012, *A&A*, 547, A51
 Hall, N., Bradač, M., Gonzalez, A. H., et al. 2012, *ApJ*, 745, 155
 Hu, E. M., Cowie, L. L., Barger, A. J., et al. 2010, *ApJ*, 725, 394
 Hutter, A., Dayal, P., Partl, A. M., & Müller, V. 2014, *MNRAS*, 441, 2861
 Iliev, I. T., Mellema, G., Pen, U.-L., et al. 2006, *MNRAS*, 369, 1625
 Jensen, H., Datta, K. K., Mellema, G., et al. 2013a, *MNRAS*, 435, 460
 Jensen, H., Laursen, P., Mellema, G., et al. 2013b, *MNRAS*, 428, 1366
 Kashikawa, N., Shimasaku, K., Matsuda, Y., et al. 2011, *ApJ*, 734, 119
 Kuhlen, M., & Faucher-Giguère, C.-A. 2012, *MNRAS*, 423, 862
 Loeb, A., & Rybicki, G. B. 1999, *ApJ*, 524, 527
 Malhotra, S., & Rhoads, J. E. 2006, *ApJL*, 647, L95
 McLure, R. J., Dunlop, J. S., Cirasuolo, M., et al. 2010, *MNRAS*, 403, 960
 McQuinn, M., Lidz, A., Zahn, O., et al. 2007, *MNRAS*, 377, 1043
 McQuinn, M., Lidz, A., Zaldarriaga, M., Hernquist, L., & Dutta, S. 2008, *MNRAS*, 388, 1101
 Mesinger, A., Aykatalp, A., Vanzella, E., et al. 2014., arXiv:1406.6373
 Mesinger, A., & Furlanetto, S. 2007, *ApJ*, 669, 663
 Mesinger, A., & Furlanetto, S. R. 2008, *MNRAS*, 386, 1990
 Miralda-Escudé, J., & Rees, M. J. 1998, *ApJ*, 497, 21
 Nestor, D. B., Shapley, A. E., Kornei, K. A., Steidel, C. C., & Siana, B. 2013, *ApJ*, 765, 47
 Ono, Y., Ouchi, M., Mobasher, B., et al. 2012, *ApJ*, 744, 83
 Ota, K., Iye, M., Kashikawa, N., et al. 2008, *ApJ*, 677, 12
 Ouchi, M., Shimasaku, K., Furusawa, H., et al. 2010, *ApJ*, 723, 869
 Pentericci, L., Fontana, A., Vanzella, E., et al. 2011, *ApJ*, 743, 132
 Raskutti, S., Bolton, J. S., Wyithe, J. S. B., & Becker, G. D. 2012, *MNRAS*, 421, 1969
 Santos, M. R. 2004, *MNRAS*, 349, 1137
 Santos, M. R., Ellis, R. S., Kneib, J.-P., Richard, J., & Kuijken, K. 2004, *ApJ*, 606, 683
 Schenker, M. A., Ellis, R. S., Konidaris, N. P., & Stark, D. P. 2014, arXiv:1404.4632
 Schenker, M. A., Stark, D. P., Ellis, R. S., et al. 2012, *ApJ*, 744, 179
 Schmidt, K. B., Treu, T., Trenti, M., et al. 2014, *ApJ*, 786, 57
 Siana, B., Teplitz, H. I., Ferguson, H. C., et al. 2010, *ApJ*, 723, 241
 Sobacchi, E., & Mesinger, A. 2013, *MNRAS*, 432, 3340
 Sobacchi, E., & Mesinger, A. 2014, *MNRAS*, 440, 1662
 Stark, D. P., Ellis, R. S., Chiu, K., Ouchi, M., & Bunker, A. 2010, *MNRAS*, 408, 1628
 Stark, D. P., Ellis, R. S., & Ouchi, M. 2011, *ApJL*, 728, L2
 Taylor, J., & Lidz, A. 2014, *MNRAS*, 437, 2542
 Trac, H. Y., & Gnedin, N. Y. 2011, *ASL*, 4, 228

¹⁴ The Ly α EW-PDF is affected by a combination of f_{esc} , dust, and IGM transmission. Existing observations at a fixed redshift cannot break degeneracies between these different parameters (as shown clearly by Hutter et al. 2014). However, there is additional information in the observed redshift evolution that can place more stringent constraints (see for example Dijkstra et al. 2014).

Treu, T., Schmidt, K. B., Trenti, M., Bradley, L. D., & Stiavelli, M. 2013, [ApJL](#), **775**, L29
Treu, T., Trenti, M., Stiavelli, M., Auger, M. W., & Bradley, L. D. 2012, [ApJ](#), **747**, 27
Vanzella, E., Guo, Y., Giavalisco, M., et al. 2012, [ApJ](#), **751**, 70

Vanzella, E., Pentericci, L., Fontana, A., et al. 2011, [ApJL](#), **730**, L35
Wilkins, S. M., Bunker, A. J., Lorenzoni, S., & Caruana, J. 2011, [MNRAS](#), **411**, 23
Wilkins, S. M., Stanway, E. R., & Bremer, M. N. 2014, [MNRAS](#), **439**, 1038
Zheng, Z., Cen, R., Trac, H., & Miralda-Escudé, J. 2010, [ApJ](#), **716**, 574